Saturation Magnetization Magnetic Circular Dichroism Spectroscopy of Systems with Positive Zero-Field Splittings: Application to $FeSiF_6 \cdot 6H_2O$

Cecelia Campochiaro, Elizabeth G. Pavel, and Edward I. Solomon*

Department of Chemistry, Stanford University, Stanford, California 94305

Received March 15, 1995[⊗]

The magnetic circular dichroism (MCD) spectrum and saturation magnetization MCD data of the near-infrared d → d transitions of the hexaaquoferrous complex ferrous fluorosilicate are presented. These data are used to develop a theoretical framework for modeling saturation magnetization MCD data from randomly oriented, integer spin systems, such as ferrous metalloprotein active sites, that have positive zero-field splittings (ZFS) and hence a nondegenerate ground state. The sign of the ZFS coupled with the energies of the MCD transitions provides direct information about the energy ordering of the d-orbitals. Although ferrous fluorosilicate does not have a degenerate ground state, it exhibits increasing MCD intensity with decreasing temperature much like a Kramers system. The low-temperature MCD intensity is shown to be due to a temperature-dependent nonlinear $\mathscr{B}$-term mechanism which results from a z-polarized transition moment coupled with off-axis Zeeman effects. Since the data from a complex with positive ZFS can qualitatively resemble a system with negative ZFS, ways to distinguish the sign of the zero-field splitting from saturation magnetization MCD data are also presented. This extension of the current saturation magnetization MCD methodology to include cases with positive ZFS is important since MCD has proven to be a crucial technique for characterizing the geometric and electronic structures of mononuclear non-heme ferrous enzymes.

Introduction

Metal centers with $S > {}^1/_2$ have zero-field splittings (ZFS) that lead to interesting effects at low temperatures due to the unequal Boltzmann populations among the ground-state sublevels. In even electron systems time reversal symmetry is not present, so additional effects due to the non-Kramers behavior of the wave functions will occur and must be treated.[1] Saturation magnetization, or variable-temperature, variable-field (VTVH), magnetic circular dichroism (MCD) spectroscopy measures the MCD intensity of an optical transition at various temperatures and magnetic fields and is a powerful probe of ground-state electronic structure.[2-5] The two main advantages of VTVH MCD are that it directly probes the chromophore, unlike magnetic susceptibility which is a bulk technique, and that it can be applied to all paramagnetic species with MCD active absorption bands, unlike electron paramagnetic resonance (EPR) spectroscopy which has both selection rule ($\Delta M_S = \pm 1$ for transverse mode) and ZFS requirements ($\Delta E \leq 0.33$ for X-band) to observe transitions. These advantages have made MCD spectroscopy a key technique for understanding the geometric and electronic structures of many iron containing metalloprotein active sites, including the heme proteins,[5,6] iron–sulfur proteins,[7-9] binuclear non-heme iron proteins,[10,11] and the mononuclear non-heme iron proteins.[12-16] In particular, the $S = 2$ reduced forms of the high-spin mononuclear non-heme iron enzymes is usually not amenable to study by magnetic susceptibility or EPR, making VTVH MCD studies critically important.

These ferrous active sites have a high-spin d^6 configuration. The ^5D atomic ground state splits into $^5T_{2g}$ and ^5E_g states separated by $10Dq$, with $^5T_{2g}$ lowest for all but tetrahedral geometries. Under the influence of a low-symmetry crystal field, the $^5T_{2g}$ ground state will split into a singly degenerate $^5B_2$ state and a doubly degenerate ^5E state. The sign of the crystal field splitting is defined such that ^5E is lowest for negatively and $^5B_2$ lowest for positively signed splittings, corresponding to axial elongation or compression, respectively, along a tetragonal distortion of octahedral symmetry. If $^5B_2$ is lowest in energy, second-order spin–orbit coupling with the ^5E excited state leads to a splitting of the $S = 2$ spin manifold to give a positive axial ZFS ($+D$, *vide infra*), while if ^5E is lowest, in-state spin–orbit coupling leads to a non-Kramers doublet lowest in energy which corresponds to a negative ZFS ($-D$).

We now extend the current theoretical framework of VTVH MCD data analysis of non-Kramers systems[12] to include positive zero-field splittings and to show that an unequivocal assignment of the sign and magnitude of these splittings is possible. A

[⊗] Abstract published in *Advance ACS Abstracts,* August 1, 1995.

(1) Abragam, A.; Bleaney, B. *Electron Paramagnetic Resonance of Transition Ions*; Dover Publications, Inc.: New York, 1986.
(2) Solomon, E. I.; Zhang, Y. *Acc. Chem. Res.* **1992**, *25*, 343.
(3) Johnson, M. K. In *Metal Clusters in Proteins*; Que, L., Jr., Ed.; ACS Symposium Series 372; American Chemical Society: Washington DC, 1988; p 326.
(4) Browett, W. R.; Fucaloro, A. F.; Morgan, T. V.; Stephens, P. J. *J. Am. Chem. Soc.* **1983**, *105*, 1868.
(5) Thomson, A. J.; Johnson, M. K. *Biochem. J.* **1980**, *191*, 411.
(6) Dawson, J. H.; Dooley, D. M. In *Iron Prophyrins Part III*; Lever, A. B. P., Gray, H. B., Eds.; VCH: New York, 1985; p 93.
(7) Stephens, P. J.; Jensen, G. M.; Devlin, F. J.; Morgan, T. V.; Stout, C. D.; Martin, A. E.; Burgess, B. K. *Biochemistry* **1991**, *30*, 3200.
(8) Johnson, M. K.; Bennett, D. E.; Fee, J. A.; Sweeney, W. V. *Biochim. Biophys. Acta* **1987**, *911*, 81.
(9) Bennett, D. E.; Johnson, M. K. *Biochim. Biophys. Acta* **1987**, *911*, 71.
(10) Reem, R. C.; Solomon, E. I. *J. Am. Chem. Soc.* **1987**, *109*, 1216.
(11) Pulver, S.; Froland, W. A.; Fox, B. G.; Lipscomb, J. D.; Solomon, E. I. *J. Am. Chem. Soc.* **1993**, *115*, 12409.
(12) Whittaker, J. W.; Solomon, E. I. *J. Am. Chem. Soc.* **1988**, *110*, 5329.
(13) Mabrouk, P. A.; Orville, A. M.; Lipscomb, J. D.; Solomon, E. I. *J. Am. Chem. Soc.* **1991**, *113*, 4053.
(14) Pavel, E. G.; Martins, L. J.; Ellis, W. R., Jr.; Solomon, E. I. *Chem. Biol.* **1994**, *1*, 173.
(15) Pavlosky, M. A.; Zhang, Y.; Westre, T. E.; Gan, Q.-F.; Pavel, E. G.; Campochiaro, C.; Hedman, B.; Hodgson, K. O.; Solomon, E. I. *J. Am. Chem. Soc.* **1995**, *117*, 4316.
(16) Loeb, K. E.; Zaleski, J. M.; Westre, T. E.; Guajardo, R. J.; Mascharak, P. K.; Hedman, B.; Hodgson, K. O.; Solomon, E. I. *J. Am. Chem. Soc.* **1995**, *117*, 4545.

0020-1669/95/1334-4669$09.00/0 © 1995 American Chemical Society

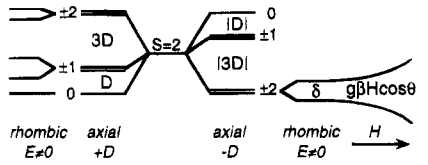

Figure 1. Degeneracy of the five $S = 2$ sublevels removed by axial (D) and rhombic (E) zero-field splittings. For $-D$ (right), the $M_S = \pm 2$ doublet is lowest in energy; rhombic ZFS separates the two components by δ and the Zeeman effect causes further splitting. For $+D$ (left), the $M_S = 0$ singlet is lowest in energy and rhombic ZFS removes the degeneracy of the $M_S = \pm 1$ and ± 2 excited states.

low-symmetry, magnetically-isolated, high-spin ferrous ion is described by the spin Hamiltonian given in eq 1, where $\tilde{\mathbf{D}}$ is

$$\mathcal{H} = \vec{S}\cdot\tilde{\mathbf{D}}\cdot\vec{S} + \beta\vec{H}\cdot\tilde{\mathbf{g}}\cdot\vec{S} \quad (1)$$

the ZFS tensor, $\vec{S}$ is the spin operator, β is the Bohr magneton, $\vec{H}$ is the applied magnetic field, and $\tilde{\mathbf{g}}$ is the g tensor. Assuming that the $\tilde{\mathbf{D}}$ and $\tilde{\mathbf{g}}$ tensors are colinear and that the total spin is two ($S = 2$), the general expression in eq 1 can be rewritten as eq 2.

$$\mathcal{H} = D(\hat{S}_z^2 - S(S+1)/3) + E(\hat{S}_x^2 - \hat{S}_y^2) + \beta(g_xH_x\hat{S}_x + g_yH_y\hat{S}_y + g_zH_z\hat{S}_z) \quad (2)$$

D and E are the axial and rhombic ZFS parameters, respectively, and g_x, g_y, and g_z are the molecular g values. The spin Hamiltonian provides a much better approximation for $+D$ than for $-D$ systems because the ^{5}B ground state is orbitally nondegenerate. At zero field and in the axial limit ($E = 0$), this Hamiltonian will define a spin ladder containing a doublet, doublet, singlet pattern ($M_S = \pm 2, \pm 1, 0$) for $-D$ (Figure 1, right) or a singlet, doublet, doublet pattern ($M_S = 0, \pm 1, \pm 2$) for $+D$ (Figure 1, left). With the inclusion of rhombic ZFS ($E \neq 0$), the $M_S = \pm 2$ doublet will split in second order by the amount δ, and the $M_S = \pm 1$ doublet will split in first order, as shown in Figure 1. Application of a magnetic field parallel to the molecular z-axis causes the lowest-energy $M_S = \pm 2$ doublet of a negative ZFS system to split with $g = 8.0$ (see Figure 1).

$-D$ systems, which have a doublet lowest, are MCD active and are well described by an isolated $M_S = \pm 2$ non-Kramers doublet model.[2,12] The MCD intensity behavior of near-infrared d → d transitions qualitatively resembles Kramers $\mathcal{C}$-term behavior[17-20] since the intensities increase with decreasing temperature and increasing magnetic field. However, the VTVH MCD intensities of the non-Kramers system are quantitatively different due to the ZFS of the two partners of the $M_S = \pm 2$ doublet (δ) and the magnetic field dependence of the non-Kramers wave functions.[12] In $+D$ systems, a nondegenerate $M_S = 0$ sublevel is lowest and therefore should not be MCD active. However, VTVH MCD on a $+D$ high-spin ferrous site was observed for the heme protein cytochrome c oxidase in 1980[5] which appeared to have $\mathcal{C}$-term dependence, but a quantitative analysis of the data was not presented. An initial attempt to treat $+D$ VTVH MCD data has been presented,[21,22] but does not describe the observed nonlinear behavior. Here we develop a model for describing VTVH MCD data of $+D$ systems using the well-characterized model complex ferrous fluorosilicate, $FeSiF_6{\cdot}6H_2O$, which has been clearly shown experimentally to have positive ZFS.[23-25]

Ferrous fluorosilicate (FFS) consists of a high-spin Fe^{2+} ion, surrounded by six water molecules in a nearly octahedral geometry, and a fluorosilicate counterion. The high-temperature ($T_c \sim 240$ K) site symmetry of FFS is D_{3d}, and the low-temperature site symmetry is nearly C_{2h}.[26] Only the low-temperature form will be considered in this paper. The axial ZFS parameter D was originally determined from single crystal magnetic susceptibility measurements to be $+10.9$ cm^{-1} using a purely axial spin Hamiltonian.[23] Far-infrared absorption allowed observation of the transitions between the $M_S = 0$ and $M_S = \pm 1$ ground state sublevels, and the full spin Hamiltonian given in eq 2 was applied to obtain $D = +11.9$ and $|E| = 0.67$ cm^{-1}.[24,27] These results were confirmed by electronic Raman studies, in which all the spin sublevels were clearly observed.[25] Thus, the spin Hamiltonian parameters of FFS are well-defined, making this an ideal complex for understanding the VTVH MCD data of a $+D$ system.

Experimental Section

Ferrous fluorosilicate was prepared anaerobically according to published procedures.[28] The pale pink microcrystalline sample was ground by hand with an agate mortar and pestle in a dry box and mixed with fluorinated grease into a mull. A mull study is preferable to a single-crystal study since biaxial crystals are unsuitable for MCD spectroscopy and a randomly oriented sample more nearly resembles frozen protein solutions, for which this methodology will ultimately be applied. MCD samples were made by pressing a fine layer of the mull between two Infrasil quartz disks. Low-temperature CD (*i.e.*, baseline) and MCD spectra were collected with a Jasco J200D spectropolarimeter equipped with an InSb detector and an Oxford SM4−7T superconducting magnet/cryostat, which is capable of generating magnetic fields up to 7 T and temperatures as low as 1.6 K. Depolarization of the mull was judged to be <5% at 10 K using established methods.[4] The MCD spectrum was corrected by subtracting zero-field and temperature-independent background signals. The corrected spectrum was fit to Gaussian bandshapes *via* a Levenberg−Marquardt algorithm.

Results

The 4.2 K single-crystal absorption spectrum of FFS (adapted from Agnetta *et al.*[29]) is shown in Figure 2A. This absorption spectrum is well-described by three Gaussians at 9600, 10 800, and 13 700 cm^{-1}. Although the 9600 and 10 800 cm^{-1} bands were not explicitly resolved by Agnetta *et al.*, a broad band at 10 580 cm^{-1} was assigned as the transition to the Jahn−Teller split ^{5}E$_g$ excited state. The 13 700 cm^{-1} band was assigned as a spin-forbidden transition from the ^{5}T$_{2g}$ ground state to a triplet state arising from the d^6 configuration.[29] The 1.6 K MCD spectrum, shown in Figure 2B, can be Gaussian fit with the same three bands as the absorption spectrum, allowing only the signs and magnitudes of the intensities to change. The ^{5}T$_{2g}$ → ^{5}E$_g$ transition appears qualitatively similar to the absorption spectrum, but the quintet → triplet transition is broader and more intense in the MCD spectrum. This result is reasonable since the MCD spectrum should reflect different components of the triplet manifold[30] because of the different selection rules for MCD vs absorption spectroscopies.[18]

(17) Stephens, P. J. *J. Chem. Phys.* **1970**, *52*, 3489.
(18) Stephens, P. J. *Annu. Rev. Phys. Chem.* **1974**, *25*, 201.
(19) Stephens, P. J. *Adv. Chem. Phys.* **1976**, *35*, 197.
(20) Piepho, S. B.; Schatz, P. N. *Group Theory in Spectroscopy: With Applications to Magnetic Circular Dichroism*; John Wiley & Sons: New York, 1983.
(21) Collingwood, J. C.; Day, P.; Denning, R. G. *J. Chem. Soc., Faraday Trans.* **1973**, *269*, 591.
(22) Hamilton, C. L.; Scott, R. A.; Johnson, M. K. *J. Biol. Chem.* **1989**, *264*, 11605.
(23) Jackson, L. C. *Philos. Mag.* **1959**, *4*, 269.
(24) Champion, P. M.; Sievers, A. J. *J. Chem. Phys.* **1977**, *66*, 1819.
(25) Gnezdilov, V. P.; Eremenko, V. V.; Peschanskii, A. V.; Fomin, V. I. *Fiz. Nizk. Temp. (Kiev)* **1991**, *17*, 253.
(26) Price, D. C. *Can. J. Phys.* **1987**, *65*, 1280.
(27) Rubins, R. S.; Fetterman, H. R. *J. Chem. Phys.* **1979**, *71*, 5163.
(28) Hamilton, W. C. *Acta Crystallogr.* **1962**, *15*, 353.
(29) Agnetta, G.; Garofano, T.; Palma-Vittorelli, M. B.; Palma, M. U. *Philos. Mag.* **1962**, *7*, 495.
(30) Sugano, S.; Tanabe, Y.; Kamimura, H. *Multiplets of Transition-Metal Ions in Crystals*; Academic Press, Inc.: New York, 1970.

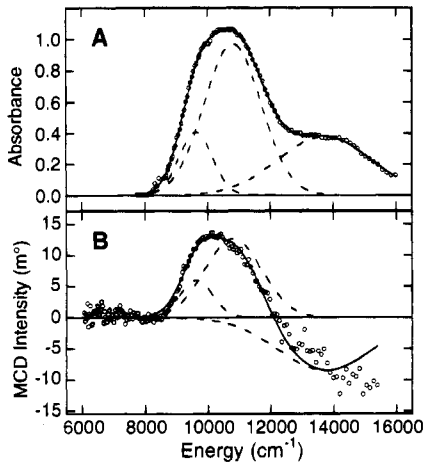

Figure 2. A. 4.2 K single crystal absorption spectrum of FFS, adapted from Agnetta *et al.*[29] B. 1.6 K, 7 T MCD spectrum of FFS, corrected for zero-field and temperature-independent background signals. Dashed lines indicate individual Gaussian components of the best simultaneous Gaussian fit (—) to the raw data (○).

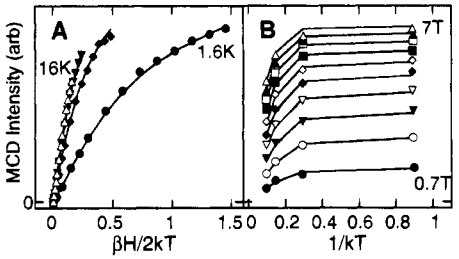

Figure 3. FFS saturation magnetization saturation data collected at 10 530 cm^{-1} plotted vs (A) $\beta H/2kT$ for 1.6 (●), 5 (◆), 10 (▼), and 16 K (△) and (B) $1/kT$ for 0.7 (●), 1.4 (○), and 2.1 T (▼), etc., in 0.7 T increments up to 7 T (△). Three-level $+D$ fit (—) to the raw data with energies fixed according to the known ZFS parameters (for $H \parallel y$). The fit was obtained by fixing $g = 8.0$ and treating A_{satlim} and B_0 as floated parameters for the pseudodoublet.

VTVH MCD data of FFS were collected at ~10 530 cm^{-1} for temperatures up to 40 K, and the 1.6, 5, 10, and 16 K data are plotted vs $\beta H/2kT$ and $1/kT$ in parts A and B of Figure 3, respectively. The $\beta H/2kT$ plot in Figure 3A is similar to others observed for ferrous metalloenzymes[12,13] and reveals a high degree of nesting (nonsuperimposing curves). The $1/kT$ plot in Figure 3B shows that the MCD intensity increases with decreasing temperature and increasing field between 16 and 5 K, but does not increase when the temperature falls from 5 to 1.6 K. While the 1.6 K MCD intensities do not saturate with field by 7 T, they are clearly approaching a saturation limit.

Analysis

In order to understand the origin of VTVH MCD intensities, it is necessary to consider the expression that defines the orientation averaged $\mathcal{C}$-term MCD intensity, $\bar{\mathcal{C}}_0$, shown in eq 3. Equation 3 consists of the dot product of a Zeeman matrix

$$\bar{\mathcal{C}}_0 = \frac{-i}{3|d_A|}\sum\langle A|\vec{\mu}|A\rangle\cdot(\langle A|\vec{m}|J\rangle \times \langle J|\vec{m}|A\rangle) \qquad (3)$$

element ($\vec{\mu} = \vec{L} + 2\vec{S}$) within a ground state doublet $|A\rangle$ and the cross product of two electric dipole matrix elements ($\vec{m} = e\vec{r}$) connecting $|A\rangle$ to an excited state $|J\rangle$.[20] d_A is the degeneracy of the ground state. Expanding eq 3 using the Cartesian components of $\vec{\mu}$ and $\vec{m}$ yields three terms, each involving the product of a Zeeman matrix element for a magnetic field along the molecular x, y, or z directions and a product of electric dipole matrix elements along y and z, x and z, or x and y, respectively. Thus, the Zeeman direction is normal to the plane defined by the electric dipole transition directions, as shown in eq 4. The

$$\mathcal{C}_0 = \frac{-i}{3|d_A|} \times Im\sum[\langle A|\mu_x|A\rangle(\langle A|m_y|J\rangle\langle J|m_z|A\rangle - \langle A|m_z|J\rangle\langle J|m_y|A\rangle) + \langle A|\mu_y|A\rangle(\langle A|m_x|J\rangle\langle J|m_z|A\rangle - \langle A|m_z|J\rangle\langle J|m_x|A\rangle) + \langle A|\mu_z|A\rangle(\langle A|m_x|J\rangle\langle J|m_y|A\rangle - \langle A|m_y|J\rangle\langle J|m_x|A\rangle)] \qquad (4)$$

last term in eq 4, with the Zeeman interaction for $H \parallel z$ and the electric dipole transition moments along x and y, usually dominates over the other two terms because the Zeeman effect is largest along the z direction and transitions to the $^5E(d_{z^2}, d_{x^2-y^2})$ excited state are xy-polarized.

As most VTVH MCD analysis has been performed on $-D$ systems, it is worthwhile to briefly consider the $-D$ model as a starting point for understanding the VTVH MCD behavior of $+D$ systems. For $H \parallel z$ and a purely xy-polarized electric dipole transition, eq 3 can be applied to a Kramers doublet to obtain an MCD intensity expression appropriate for low temperatures and high magnetic fields. This $\mathcal{C}$-term saturation expression[31] is given as eq 5. A_{satlim} is the intensity when the transition is

$$\Delta\epsilon = A_{satlim}\int_0^{\pi/2}\cos\theta\sin\theta\tanh\left(\frac{g_{||}\beta H\cos\theta}{2kT}\right)d\theta \qquad (5)$$

saturated ($\mathcal{C}$-term intensity scaling factor), θ is the angle between the applied magnetic field (H) and the molecular z-axis, β is the Bohr magneton, k is Boltzmann's constant, and T is the absolute temperature. This model was expanded to include even electron systems by adding the non-Kramers effects of ZFS (δ in cm^{-1}) and field-dependent wave functions,[12] followed by the inclusion of excited state doublets.[32] We have now adapted these results to give a general MCD intensity expression, shown in eq 6, for any zero-field-split doublet with either doublet or singlet excited states (assuming xy-polarization).

$$\Delta\epsilon = \sum_{\substack{i\\ \text{doublets}}}\left\{(A_{satlim})_i\int_0^{\pi/2}\frac{\cos^2\theta\sin\theta}{\Gamma_i}g_{||i}\beta H\,\alpha_i\,d\theta + B_iH\gamma_i\right\} + \sum_{\substack{m\\ \text{singlets}}}B_mH\eta_m \qquad (6)$$

where

$$\Gamma_i = \sqrt{ZFS_i^2 + (g_{||i}\beta H\cos\theta)^2}$$

$$\alpha_i = \frac{(e^{-(E_i-\Gamma_i/2)/kT} - e^{-(E_i+\Gamma_i/2)/kT})}{\sum_{\substack{j\\ \text{doublets}}}(e^{-(E_j-\Gamma_j/2)/kT} + e^{-(E_j+\Gamma_j/2)/kT}) + \sum_{\substack{n\\ \text{singlets}}}(e^{-E_n/kT})}$$

$$\gamma_i = \frac{(e^{-(E_i-ZFS_i/2)/kT} + e^{-(E_i+ZFS_i/2)/kT})}{\sum_{\substack{j\\ \text{doublets}}}(e^{-(E_j-ZFS_j/2)/kT} + e^{-(E_j+ZFS_j/2)/kT}) + \sum_{\substack{n\\ \text{singlets}}}(e^{-E_n/kT})}$$

$$\eta_m = \frac{(e^{-E_m/kT})}{\sum_{\substack{j\\ \text{doublets}}}(e^{-(E_j-ZFS_j/2)/kT} + e^{-(E_j+ZFS_j/2)/kT}) + \sum_{\substack{n\\ \text{singlets}}}(e^{-E_n/kT})}$$

The second half of eq 6 includes the effects of temperature-

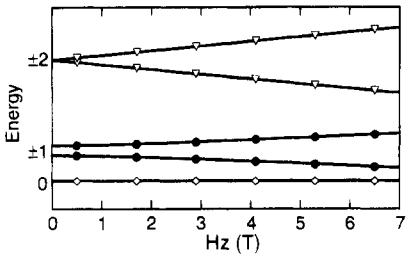

Figure 4. Energies of the $S = 2$ sublevels, $M_S = 0$ (◇), ±1 (●), and ±2 (▽), plotted as a function of magnetic field for $H \parallel z$.

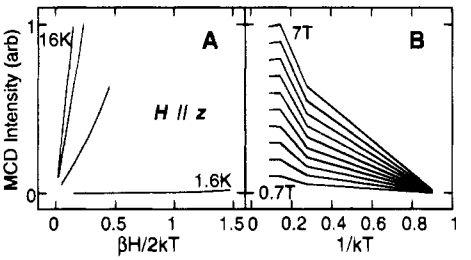

Figure 5. Variable-temperature, variable-field MCD data (calculated from the spin Hamiltonian for a $+D$, $S = 2$ manifold with $H \parallel z$) plotted vs (A) $\beta H/2kT$ and (B) $1/kT$. The energies of the spin sublevels were fixed according to the known ZFS parameters for FFS. Simulated data were calculated using $g_{\parallel} = 0.0$, 4.0, 8.0 and $A_{\text{satlim}} = 0.0$, 1.0, 1.0 for the $M_S = 0$, ±1, and ±2 sublevels, respectively; linear $\mathcal{B}$-terms were excluded. Data were calculated for 1.6, 5, 10, and 16 K and for fields from 0.7 to 7.0 T, in 0.7 T increments.

independent linear $\mathcal{B}$-terms, where B is the magnitude of the $\mathcal{B}$-term intensity reported as a percent of the $\mathcal{C}$-term intensity ($A_{\text{satlim}i}$). The parameters ZFS_i, $g_{\parallel i}$, and $A_{\text{satlim}i}$ are defined for each of the i doublets, and $B_{i/m}$ is defined for each doublet/singlet. $E_{i/m}$ is the energy of the i/mth doublet/singlet state above the ground state ($E_{GS} \equiv 0.0$). For the $-D$ case, ZFS_i is equal to δ from Figure 1. Equation 6 can be iteratively fit to VTVH MCD data (magnetic field, absolute temperature, observed MCD intensity) using a least squares algorithm. The $-D$ spin manifold is constructed by assigning a doublet $g_{\parallel} \approx 8$ ($M_S = \pm 2$) ground state, followed at higher energy by a doublet $g_{\parallel} \approx 4$ ($M_S = \pm 1$) excited state and a singlet ($M_S = 0$) excited state. The $+D$ spin manifold is similarly constructed by placing these states in the opposite energy order.

In the $+D$ case, the lowest-energy sublevel is nondegenerate and no $\mathcal{C}$-term intensity is expected, yet MCD intensity has been observed at low temperatures. Such a case was considered by Collingwood *et al.*,[21] who argued that two nondegenerate levels could exhibit $\mathcal{C}$-term-like behavior if a nonzero Zeeman matrix element existed between them, according to eq 7. This

$$\mathcal{B} = \frac{3}{|d_A|}\langle K|\mu_z|A\rangle(\langle A|m_+|J\rangle\langle J|m_-|K\rangle - \langle A|m_-|J\rangle\langle J|m_+|K\rangle)\tanh\left(\frac{\Delta E_{KA}}{2kT}\right) \quad (7)$$

temperature-dependent $\mathcal{B}$-term equation describes the MCD intensity resulting from a two-level system consisting of the nondegenerate levels $|A\rangle$ and $|K\rangle$ which interact *via* a Zeeman interaction for $H \parallel z$ and exhibit only xy-polarized electric dipole transitions to the excited states probed. In eq 7, μ_z is the Zeeman operator connecting $|A\rangle$ and $|K\rangle$, $m_{\pm}$ are the xy-polarized electric dipole transition moments from the ground-state sublevels to the excited state $|J\rangle$, and ΔE_{KA} is the ZFS. Equation 7 is very similar to the standard $\mathcal{C}$-term expression, and, in fact, Collingwood *et al.* show that the saturation behavior of a temperature-dependent $\mathcal{B}$-term is identical to that of a $\mathcal{C}$-term except that ΔE is substituted for the Zeeman splitting, $g\beta H$. However, this treatment omits the effect of the Zeeman operator on the energies of states $|A\rangle$ and $|K\rangle$. A second $+D$ MCD study applied eq 7 to fit the temperature-dependent VTVH data of a $+D$ Ni^{2+} enzyme;[22] however, the wave functions were treated as field-independent, which is an oversimplification.

***xy*-Polarized Transitions.** The spin Hamiltonian given in eq 2 has been used to calculate the energy level diagram of FFS under the effects of a magnetic field applied along the molecular z-axis, using the established parameters $D = 11.9$ and $E = 0.67$ cm^{-1}. The resulting diagram (Figure 4) shows that the lowest-energy sublevel is invariant with respect to magnetic field; therefore the $M_S = 0$ singlet has no Zeeman interactions with other sublevels and cannot contribute any MCD intensity. However, the $M_S = \pm 1$ and $M_S = \pm 2$ doublets can contribute MCD intensity according to the Boltzmann populations of their respective partners. Equation 6 was applied to a $+D$ spin manifold ($M_S = 0$, ±1, ±2 in increasing energy as described above) to simulate VTVH MCD behavior for a $+D$ system with pure xy-polarization. The resulting calculated data are plotted vs $\beta H/2kT$ and $1/kT$ in parts A and B of Figure 5, respectively. As expected, the MCD intensity is zero at low temperatures, when only the $M_S = 0$ state is populated, and increases as the high-energy doublets begin to be populated. However, this behavior is unlike the VTVH MCD behavior observed for FFS (Figure 3) in that the FFS data has maximum intensity at lowest temperature, and therefore other contributions to the MCD intensity must be considered.

***z*-Polarized Transitions.** If a magnetic field is applied along the x or y molecular axes, the resulting energy level diagrams calculated for FFS using eq 2 are very different from that for the $H \parallel z$ case. For $H \parallel x$ (Figure 6A), the $M_S = 0$ sublevel interacts *via* a first-order Zeeman effect with the higher-energy partner of the $M_S = \pm 1$ doublet, while the lower-energy partner of the $M_S = \pm 1$ doublet is almost invariant to field. A similar diagram is produced for $H \parallel y$ (Figure 6C), except that now the $M_S = 0$ sublevel interacts *via* a first-order Zeeman effect with the lower-energy partner of the $M_S = \pm 1$ doublet, and the higher-energy partner of the $M_S = \pm 1$ doublet is nearly field-invariant. In both cases the $M_S = \pm 2$ doublet is essentially field independent.

To understand the importance of these off-axis Zeeman effects on the MCD intensity of FFS, the Zeeman effect for $H \parallel x$ is considered in more detail below. Equation 8 relates the components of the $\tilde{\mathbf{D}}$ tensor to the ZFS parameters D and E.[1]

$$\tilde{\mathbf{D}} = \begin{pmatrix} D_x & 0 & 0 \\ 0 & D_y & 0 \\ 0 & 0 & D_z \end{pmatrix} = \begin{pmatrix} -D/3 + E & 0 & 0 \\ 0 & -D/3 - E & 0 \\ 0 & 0 & 2D/3 \end{pmatrix} \quad (8)$$

The spin Hamiltonian expression given in eq 1 can be rewritten in terms of the diagonal components of the $\tilde{\mathbf{D}}$ tensor to give eq 9. This form of the spin Hamiltonian presumes that both the

$$\mathcal{H} = D_x\hat{S}_x^2 + D_y\hat{S}_y^2 + D_z\hat{S}_z^2 + \beta(g_xH_x\hat{S}_x + g_yH_y\hat{S}_y + g_zH_z\hat{S}_z) \quad (9)$$

$\tilde{\mathbf{D}}$ and $\tilde{\mathbf{g}}$ tensors are quantized along the molecular z-axis and that the eigenvectors have the usual spin labels of $M_S = 0$, ±1, and ±2. Requantizing the $\tilde{\mathbf{D}}$ tensor along the molecular x-axis is achieved by mapping D_x, D_y, and D_z into D_z, D_x, and D_y, respectively, and relabeling the new axes x', y', and z', so that x in the original coordinate system is now z'. This transformation results in new spin labels for the zero-field wave functions.

(31) Buckingham, A. D.; Stephens, P. J. *Annu. Rev. Phys. Chem.* **1966**, *17*, 399.
(32) McCormick, J. M. Ph.D. Thesis, Stanford University, 1991.

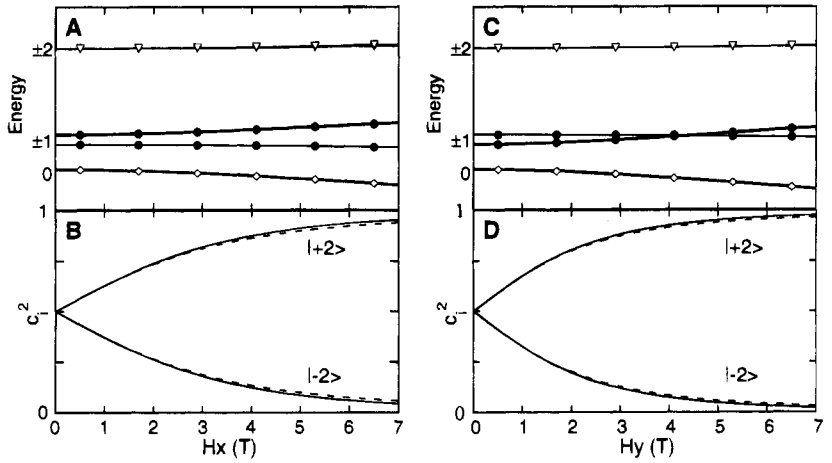

Figure 6. A. Energies of the $S = 2$ sublevels, $M_S = 0$ (◇), ±1 (●), and ±2 (▽), plotted as a function of magnetic field for $H \parallel x$. B. Coefficients c_i^2 of the $|\pm 2\rangle^{z'}$ components of the $|0\rangle^z$ ground state (—) are compared with those of a pure $M_S = \pm 2$ non-Kramers doublet with the same ZFS and g-value (- - -). C and D. Same as parts A and B but for $H \parallel y$.

The wave function coefficients have been calculated for FFS using $D = 11.9$ and $E = 0.67$ cm^{-1} and are given in eq 10, where the superscript z refers to the z-quantized $\tilde{\mathbf{D}}$ tensor and z' to the x-quantized $\tilde{\mathbf{D}}$ tensor.

$$|0\rangle^z \rightarrow +0.59|+2\rangle^{z'} + 0.59|-2\rangle^{z'} - 0.54|0\rangle^{z'}$$

$$|-1\rangle^z \rightarrow -0.71|+1\rangle^{z'} + 0.71|-1\rangle^{z'}$$

$$|+1\rangle^z \rightarrow -0.71|+2\rangle^{z'} + 0.71|-2\rangle^{z'}$$

$$|-2\rangle^z \rightarrow +0.71|+1\rangle^{z'} + 0.71|-1\rangle^{z'}$$

$$|+2\rangle^z \rightarrow +0.38|+2\rangle^{z'} + 0.38|-2\rangle^{z'} - 0.84|0\rangle^{z'} \quad (10)$$

From both Figure 6A and eq 10, it is clear that *the $M_S = 0$ level and the higher-energy partner of the $M_S = \pm 1$ pair behave very similarly to an $M_{S'} = \pm 2$ non-Kramers doublet,* where g(effective) = 8.0 and δ is the ZFS between those two levels, which in the case of FFS with $H \parallel x$ is 13.9 cm^{-1}. This is illustrated in Figure 6B, which shows the coefficients c_i^2 of the $|\pm 2\rangle^{z'}$components of $|0\rangle^z$ (solid lines) compared with those of a pure $M_S = \pm 2$ non-Kramers doublet with the same ZFS and g value (dashed lines). An analogous situation occurs for $H \parallel y$ (Figure 6D), except that the effective ZFS of the Zeeman active levels is 9.9 cm^{-1}, rather then 13.9 cm^{-1}. *The VTVH MCD behavior for $H \parallel x$ (or y) can thus be described by a three-level model with a pseudodoublet ground state split by the amount ZFS $\approx D + 3E$ cm^{-1} ($D - 3E$ cm^{-1} for $H \parallel y$), analogous to a non-Kramers doublet with the splitting δ, and a singlet excited state which is MCD-inactive and lies at $\sim D - 3E$ cm^{-1} ($D + 3E$ cm^{-1} for $H \parallel y$) above the ground state.* Simulated saturation magnetization data for these scenarios have been calculated using eq 6 and are plotted vs $\beta H/2kT$ and $1/kT$, respectively, in parts A and B of Figure 7 for $H \parallel x$ and parts C and D of Figure 7 for $H \parallel y$. The VTVH data are more linear (*i.e.*, less saturated) in the $\beta H/2kT$ plot and saturate at slightly higher temperature in the $1/kT$ plot for $H \parallel x$ than for $H \parallel y$ because the effective ZFS of the psuedodoublet is larger for H along the x direction (13.9 vs 9.9 cm^{-1}). Importantly, both of the simulated data sets in Figure 7 resemble the observed FFS data in Figure 3. It is also important to note that the curves are not linear, in contrast to the behavior predicted by Hamilton *et al.*[22]

The FFS VTVH data from Figure 3 were quantitatively fit to the $H \parallel y$ three-level model using eq 6. The known values of D and E were used to generate the ZFS of the ground-state

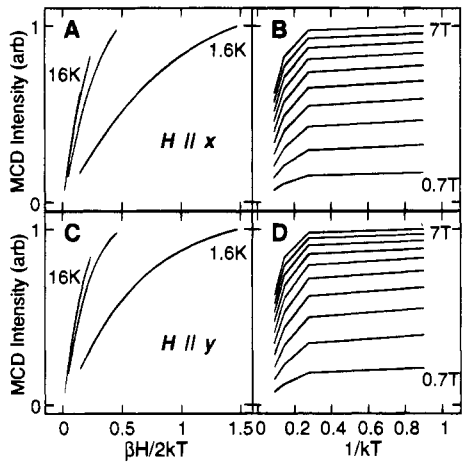

Figure 7. Variable-temperature, variable-field MCD data (calculated from the spin Hamiltonian for a $+D$, $S = 2$ manifold) plotted vs $\beta H/2kT$ and $1/kT$ for $H \parallel x$ (A and B) and $H \parallel y$ (C and D). The energies of the spin sublevels were fixed according to the known ZFS parameters for FFS. Simulation conditions are the same as those given in Figure 5.

doublet and the energy of the excited state singlet. Fixing both of these energies and keeping the g-value of the ground state at 8.0, the best fit to the data was obtained by treating A_{satlim} and B_0 of the ground state as floated parameters (assuming no significant linear $\mathcal{B}$-term contribution from the singlet). The resulting ground-state $\mathcal{B}$-term contribution was <1% and can therefore be excluded as a large contributor to the MCD intensity. The best fit to the data, shown as solid lines in parts A and B of Figure 3, provides an excellent description of the observed data and confirms that a three-level model is necessary to describe the FFS saturation magnetization behavior. In the case of metalloenzyme data, the energies of the spin Hamiltonian sublevels would be unknown; thus the three-level model must be used to fit the data if the ground-state ZFS and energy of the singlet excited state are treated as floated parameters. To verify this, another fit of the FFS data to eq 6 was performed allowing these energies plus A_{satlim} and B_0 of the ground state to vary. The resulting energies were 0, 10, and 16 cm^{-1}, which are in good agreement with the actual splittings of 0, 9.9, and 13.9 cm^{-1}. If a $-D$ model is assumed and the VTVH MCD data are fit to an isolated non-Kramers doublet with B_0, A_{satlim}, $g_{||}$, and δ treated as adjustable parameters, the data is quantitatively well described. However, the resulting best-fit parameters are unphysical: $g_{||} = 6.7$ is too low ($g_{||}$ cannot significantly deviate from 8.0 unless the system is truly $-D$, in which case

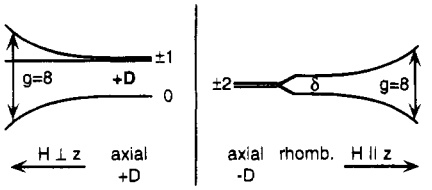

Figure 8. The dominant Zeeman effects for $+D$ and $-D$ systems are compared. For $-D$ (right), the ground state doublet is rhombically split by δ and the Zeeman effect gives $g = 8$ for $H \parallel z$, producing a $\mathcal{C}$-term intensity mechanism. For $+D$ (left), the Zeeman effect gives $g = 8$ for $H \perp z$ and couples the $M_S = 0$ sublevel with one partner of the $M_S = \pm 1$ pair, producing a temperature-dependent nonlinear $\mathcal{B}$-term intensity mechanism. The effective ZFS for $+D$ systems is expected to be larger than for $-D$ systems, on the order of $+D$ ($\pm 3E$ if rhombic ZFS is included) compared to $\delta < 7$ cm^{-1}.

deviations are to higher values[12]) and $\delta = 9$ cm^{-1} is above the range of values calculated from a full $^5T_{2g}$ Hamiltonian model ($\delta < 7$ cm^{-1}).

Discussion

The above analysis shows that the VTVH MCD data from a $+D$ system exhibit nesting, nonlinear field dependence, and increased intensity with decreasing temperature. These observations are not predicted when only $H \parallel z$ and xy-polarized electric dipole transitions are considered; however this behavior is clearly understood when the effects of off-axis Zeeman terms are included. The experimental FFS saturation magnetization data are well-described by a three-level $+D$ model composed of the lowest-energy $M_S = 0$ sublevel and the $M_S = \pm 1$ pair at $\sim D$ cm^{-1} above: $M_S = 0$ and one component of $M_S = \pm 1$ act as a pseudododoublet split by $\sim D \pm 3E$ with $g = 8$ and the other component of $M_S = \pm 1$ is an MCD-inactive excited state. An excellent fit to the FFS VTVH MCD data is obtained using the three-level model with energies based on the known ZFS parameters. If the energy spacings are not assumed, a three-level $+D$ fit returns energies in good agreement with the known values. Although the FFS data can be quantitatively fit with the $-D$ model, the resulting parameters are unphysical and argue against a $-D$ assignment.

The three-level $+D$ model is closely related to the $-D$ non-Kramers doublet model, but is fundamentally different since the origin of the $+D$ MCD intensity is a temperature-dependent $\mathcal{B}$-term, rather than a $\mathcal{C}$-term. Figure 8 summarizes the dominant Zeeman effects on the $S = 2$ spin manifold for positive and negative ZFS at the axial limit and shows the qualitative differences between the two cases. For $-D$ (Figure 8, right), MCD intensity is due to a $\mathcal{C}$-term originating from a non-Kramers $M_S = \pm 2$ doublet which is rhombically split by the amount δ and which has a $g \approx 9$ for $H \parallel z$. (g is larger than 8 because the ^5E ground state for $-D$ has in-state orbital angular momentum and must be treated by the full $^5T_{2g}$ Hamiltonian.[12]) For $+D$ (Figure 8, left), MCD intensity is due to a temperature- and field-dependent $\mathcal{B}$-term originating from an off-axis Zeeman interaction between the $M_S = 0$ and one partner of the $M_S = \pm 1$ sublevels with a ZFS $= D$. A near-axial treatment is sufficient for FFS, which has an E/D ratio of ~ 0.06; however, most ferrous complexes will exhibit larger rhombic distortions, particularly enzyme systems which have inherently low-symmetries.

Figure 9 summarizes the effects of rhombicity on systems with both positive and negative zero-field splittings. As stated above, at the axial limit a positive zero-field splitting pattern will have a nondegenerate state lowest in energy with a doublet at D cm^{-1} (Figure 9, top, left side), and MCD intensity will originate from an off-axis temperature-dependent $\mathcal{B}$-term between the lowest singlet and one partner of the $M_S = \pm 1$

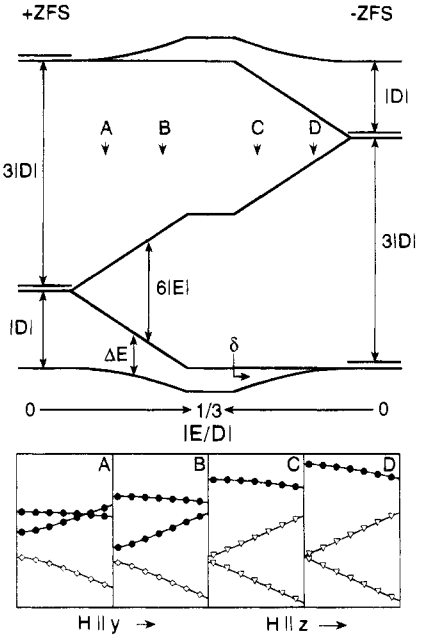

Figure 9. Effect of increasing rhombicity for both +ZFS and −ZFS $S = 2$ systems. Top: Energy levels at the axial limit for the spin Hamiltonian with +ZFS (left) and −ZFS (right). Moving toward the center of the diagram from both sides, the value of $|E|$ is increased until the ratio $|E/D|$ is at the rhomic limit of $^1/_3$. At the rhombic limit, the energy levels are symmetrically spaced in a 2−1−2 pattern. For +ZFS systems (left) the splitting pattern begins with the $M_S = 0$ singlet followed by the $M_S = \pm 1$ doublet at the axial limit, but evolves into an isolated pseudododoublet with increasing $|E|$ (center). In contrast, for −ZFS systems (right) the splitting pattern begins with the isolated $M_S = \pm 2$ doublet, which is degenerate at the axial limit and is maximally split by δ at the rhombic limit (center). Positions A, B, C, and D indicated by arrows correspond to +ZFS, $E/D = 0.10$; +ZFS, $E/D = 0.25$; −ZFS, $E/D = 0.25$; −ZFS, $E/D = 0.10$. Bottom: Field dependence of the lowest three energy levels ($M_S = 0$ (◇), ± 1 (●), ± 2 (△)) at each position A, B, C, and D with $H \parallel y$ for +ZFS and $H \parallel z$ for −ZFS.

doublet. As the magnitude of the rhombic ZFS parameter E increases, the $M_S = \pm 1$ doublet will split by $6|E|$ and the largest Zeeman interaction will be between the $M_S = 0$ level and the lower-energy component of the $M_S = \pm 1$ doublet at $\Delta E \approx D - 3|E|$ cm^{-1} for $H \parallel y$ (Figure 9, region A). As $|E|$ approaches the rhombic limit, the splitting of the $M_S = \pm 1$ doublet becomes significantly larger than ΔE and the system behaves like an isolated non-Kramer's doublet (Figure 9, region B).

Conversely, a negative zero-field splitting pattern at the axial limit will have a degenerate $M_S = \pm 2$ level lowest in energy (Figure 9, top, right side), and MCD $\mathcal{C}$-term intensity will originate from this doublet. As the magnitude of the rhombic ZFS parameter E increases, the $M_S = \pm 2$ doublet will be split in second order by an amount δ cm^{-1} and will continue to be seperated from the $M_S = \pm 1$ and $M_S = 0$ levels by $\sim 3|D| \pm 3|E|$ and $\sim 4\ |D|$, respectively (Figure 9, region D). As $|E|$ approaches the rhombic limit, the magnitude of δ increases, but the $M_S = \pm 2$ doublet is still well isolated from the higher energy levels (Figure 9, region C).

At the rhombic limit, the spin Hamiltonian dictates that the splitting between the $M_S = 0$ sublevel and the lower-energy component of the $M_S = \pm 1$ and the $M_S = \pm 2$ doublet splitting will be equal so that the only difference between +ZFS and −ZFS at the rhombic limit is the labeling of the symmetrically-spaced levels (Figure 9, center). From Figure 9 it is also clear that a rhombic system should behave according to the $-D$ model with a large value of δ. If a system is nearly rhombic, deciding whether D is positive or negative can be difficult, but is often not critical. At the rhombic limit, application of the three-level

$+D$ model may not improve the fit, and the energy of the third level should be at the upper range of kT for the experimental data. Reference 12 provides an upper limit for δ at the rhombic limit of ~ 7 cm^{-1}, so an experimentally determined value of $\delta > 7$ cm^{-1} implies that the system has +ZFS.

Thus when approaching VTVH MCD data from a structurally undefined ferrous complex, three categories must be explored: (1) axial to midrhombic $-D$, (2) axial to midrhombic $+D$, and (3) midrhombic to fully rhombic. If the best fit using the $-D$ non-Kramers doublet model returns δ or g values which are unphysical,[12] then the three-level $+D$ model is applied to see if the addition of an MCD-inactive singlet excited state provides a good description of the data. If the energy obtained for the excited state singlet is out of the thermal energy range of the experiment, the system may be near the rhombic limit. A caveat occurs if the polarization of the electric dipole transition is strongly mixed. Because the $H \parallel y$ model best described the FFS data, the ligand field transition used for the MCD data is dominantly xz-polarized and the Zeeman effect is expected to be larger for a magnetic field along y, rather than x or z. Although in practice one polarization should dominate, other $+D$ systems may exhibit VTVH MCD data that have contributions from yz-, xz-, and xy-polarizations (corresponding to Zeeman interactions for $H \parallel x$, y, and z, respectively). In such cases, a three-level model which assumes just one polarization may not accurately describe the data, but instead simultaneous fits to eq 6 for $H \parallel x$, y, and z must be performed and weighted according to the dipole polarization ratios. Additionally, if VTVH MCD data are obtained at high temperatures, the $+D$ analysis must be extended to include effects of thermally populating the $M_S = \pm 2$ doublet excited state.

Acknowledgment. This work was supported by the National Institutes of Health (GM 40392). C.C. would like to thank the National Institutes of Health for a Postdoctoral Fellowship (No. 3F32GM14428).

IC950307C